Omnipresence of the sensorimotor-association axis topography in the human connectome

Karl-Heinz Nenning, Ting Xu, Alexandre R Franco, Khena M Swallow, Arielle Tambini, Daniel S Margulies, Jonathan Smallwood, Stanley J Colcombe, Michael P Milham

NeuroImage 272 (2023) 120059

Contents lists available at ScienceDirect

NeuroImage

journal homepage: www.elsevier.com/locate/neuroimage

Omnipresence of the sensorimotor-association axis topography in the human connectome

Karl-Heinz Nenning[a,*], Ting Xu[b], Alexandre R. Franco[a,b,f], Khena M. Swallow[c], Arielle Tambini[a,f], Daniel S. Margulies[d], Jonathan Smallwood[e], Stanley J. Colcombe[a,f], Michael P. Milham[a,b]

[a] Nathan S. Kline Institute for Psychiatric Research, Orangeburg, NY, United States
[b] Child Mind Institute, New York, NY, United States
[c] Cornell University, Ithaca, NY, United States
[d] CNRS and Université de Paris, Paris, France
[e] Queen's University, Kingston, Ontario, Canada
[f] New York University, New York, NY, United States

ARTICLE INFO

Keywords:
Connectivity gradients
Somatosensory-association axis
Individual differences
Weak connections
Resting-state fMRI

ABSTRACT

Low-dimensional representations are increasingly used to study meaningful organizational principles within the human brain. Most notably, the sensorimotor-association axis consistently explains the most variance in the human connectome as its so-called principal gradient, suggesting that it represents a fundamental organizational principle. While recent work indicates these low dimensional representations are relatively robust, they are limited by modeling only certain aspects of the functional connectivity structure. To date, the majority of studies have restricted these approaches to the strongest connections in the brain, treating weaker or negative connections as noise despite evidence of meaningful structure among them. The present work examines connectivity gradients of the human connectome across a full range of connectivity strengths and explores the implications for outcomes of individual differences, identifying potential dependencies on thresholds and opportunities to improve prediction tasks. Interestingly, the sensorimotor-association axis emerged as the principal gradient of the human connectome across the entire range of connectivity levels. Moreover, the principal gradient of connections at intermediate strengths encoded individual differences, better followed individual-specific anatomical features, and was also more predictive of intelligence. Taken together, our results add to evidence of the sensorimotor-association axis as a fundamental principle of the brain's functional organization, since it is evident even in the connectivity structure of more lenient connectivity thresholds. These more loosely coupled connections further appear to contain valuable and potentially important information that could be used to improve our understanding of individual differences, diagnosis, and the prediction of treatment outcomes.

1. Introduction

Dimensionality reduction techniques are increasingly utilized to uncover meaningful organizational principles of the brain. Their central assumption is that the latent connectivity structure of high-dimensional neuroimaging data can be captured in a low-dimensional space. The dimensions of such a space, referred to as connectivity gradients, have been shown to be meaningful (Glomb et al., 2021; Huntenburg et al., 2018; Margulies et al., 2016; Waymel et al., 2020), and were successfully used to study variations across individuals and species, in health and disease (Brown et al., 2022; Caciagli et al., 2022; Dong et al., 2021a; Guell et al., 2018; Hong et al., 2019; Larivière et al., 2020a; Li et al., 2021; Meng et al., 2021; Mulders et al., 2022; Nenning et al., 2017; Paquola et al., 2019; Park et al., 2022; Pasquini et al., 2022; Samara et al., 2023; Xu et al., 2020). Most notably, the sensorimotor-association axis (SA-axis), a defining feature of cortical hierarchy (Hutchinson and Barrett, 2019; Sydnor et al., 2021), has been consistently identified to explain most of the variance in the human connectome, thus referred to as the principal gradient (Margulies et al., 2016). While different mathematical approaches have been introduced to establish such a low-dimensional representation (Atasoy et al., 2016; Haak et al., 2018; Hong et al., 2020; Langs et al., 2015; Nenning et al., 2020; Vos de Wael et al., 2020), conceptual commonalities in modeling the connectome exist. To date, the majority of studies have lim-

* Corresponding author.
E-mail address: karl-heinz.nenning@nki.rfmh.org (K.-H. Nenning).

https://doi.org/10.1016/j.neuroimage.2023.120059.
Received 21 December 2022; Received in revised form 4 March 2023; Accepted 27 March 2023
Available online 30 March 2023.

ited connectivity gradient analysis to the strongest positive connections. They have a better signal-to-noise ratio and are usually considered as less noisy at the individual level; thresholding emphasizes the connectivity structure of interest and presumably removes spurious connections. Also, a growing number of studies have demonstrated that the connectivity gradients of the strongest connections characterize meaningful organizational principles (Haak et al., 2018; Hong et al., 2019; Huntenburg et al., 2018; Margulies et al., 2016; Xu et al., 2020). However, restricting analyses to the strongest edges might neglect potentially meaningful information in more loosely coupled connections, and overlook variability across individuals that characterizes individual differences. While considering only the strongest connections has its justification, it raises at least two questions: (i) How persistent are these macroscale gradients when examining a range of connectivity strengths? and (ii) What are we missing by ignoring the remaining connections?

The strongest functional connections in the brain characterize a basic scaffolding of the functional organization. They are typically found between core regions of networks (Honey et al., 2007), within the same functional networks (Gordon et al., 2017; Yeo et al., 2011), or follow homotopic connectivities (Gee et al., 2011; Stark et al., 2008). The strongest functional connections also align with actual structural connectivity (Hermundstad et al., 2013; Honey et al., 2009). But there is also evidence that less tightly coupled connections can provide meaningful information. For example, in sociology, the importance of weak connections has been widely acknowledged with the "strength of weak ties" concept (Granovetter, 1973). By looking at information spread through social networks, this theory assigns value to weaker connections as they are more variable and thus more likely to provide new information than stronger connections, which behave in a more consistent manner. Similarly, in brain networks, the non-random placement of weak connections has been shown to be important for network cohesion in macaques (Goulas et al., 2015), and crucial for the coexistence of modular specialization and global integration of brain regions (Gallos et al., 2012). Also, individual-level measures such as intelligence are more highly associated with connections that are weaker, indicating their importance to understanding human cognition (Santarnecchi et al., 2014). Previous studies have demonstrated that more loosely coupled connections tend to be located at regional borders and are more variable across individuals - often averaging to zero at the group-level (Adelstein et al., 2011; Di Martino et al., 2009; Mueller et al., 2013; Seitzman et al., 2019), characterizing transition zones between cortical systems (Cohen et al., 2008; Mennes et al., 2010). They were also observed to coincide with long-distance connections, preserving cortical interconnectedness (Markov et al., 2013), relating to sporadic between-network communication (Yang et al., 2014), and spatial properties of cortical traveling waves (Raut et al., 2021).

To address the potential value of typically neglected functional connections within the connectome, we had several key objectives. First, we systematically compared principal gradients calculated from distinct, equally sized, subsets (i.e., bins) of connections defined by their connectivity strengths and directions. Individual principal gradients were calculated for bin-specific connectivity strengths ranging from the top ranked connections ('functional affinity') at one extreme, to the bottom ranked connections ('functional enmity') on the other. Then, we used cluster analysis to sort regions based on their patterns of covariation across principal gradients calculated at different connectivity strengths. To establish the implications of connectivity strength-specific gradients and their utility in characterizing individual differences, we: (i) measured inter- and intra-bin agreement (i.e., reliability) of individual differences (vertex-level, cortex-level), and (ii) assessed the relative predictive value of the strength-specific gradients for variables such as age, sex, and full-scale intelligence quotient (FSIQ). To accomplish these objectives, we leveraged two independent datasets. The analytic workflow is outlined in Table 1.

2. Methods

2.1. Datasets

Resting-state fMRI data from two openly available datasets were used: the Human Connectome Project (HCP) (Van Essen et al., 2013), and the enhanced Nathan Kline Institute-Rockland Sample (NKI-RS) (Nooner et al., 2012). Both group- and individual-level functional connectomes were examined to probe the functional organization across a full range of connectivity thresholds.

The HCP data was acquired at Washington University at St. Louis on a customized Connectome Skyra scanner (Siemens 3 Tesla) using a multiband sequence (Smith et al., 2013; Uğurbil et al., 2013; Van Essen et al., 2013). Resting-state fMRI was acquired with a multiband factor of 8, 2 mm isotropic resolution, and a repetition time of 0.72 s for a duration of 14.4 min, which resulted in 1200 vol per run. Participants were asked to relax, keep eyes open and fixated on a crosshair, and not to fall asleep. Four resting-state runs were collected in different sessions across two days (REST1 and REST2), where each session comprised two runs with different phase encoding directions (LR and RL). We used the minimally preprocessed fMRI data that was already provided by the HCP (Glasser et al., 2013). The resting-state data has been motion corrected, minimally spatially smoothed (2 mm), high-pass filtered (2000s cutoff), denoised for motion-related confounds and artifacts using independent component analysis (Salimi-Khorshidi et al., 2014; Smith et al., 2013), and aligned with MSMAll (Robinson et al., 2014).

At the group level, we used the dense group-average functional connectome provided by the HCP S1200 data release (*HCP 1200 Subjects Data Release Reference Manual*, 2017). In brief, this connectivity matrix was constructed from minimal preprocessed data across 1003 individuals that each had ~1 h (4 × 14.4 min) of resting-state fMRI acquisitions available. The dense connectivity matrix of size 91,282×91,282 grayordinates (59,412 cortical vertices and 31,870 subcortical voxels) was calculated based on components of an incremental group-pca and released by the HCP via the ConnectomeDB (*HCP 1200 Subjects Data Release Reference Manual*, 2017).

At individual-level, we selected the 100 unrelated subjects sample from the HCP (54F/46 M, age = 29 ± 3.7 years) and calculated the functional connectivity of two resting-state fMRI sessions (REST1_LR and REST2_LR) for each individual. To promote the generalizability of our findings to the preprocessing decision of global signal regression (GSR), we additionally applied GSR to the minimal preprocessing (Kong et al., 2021; Li et al., 2019), and both GSR and non-GSR data were used to build vertex-wise connectivity matrices calculated with Pearson's correlation (Murphy and Fox, 2017). The fsaverage4 surface space (2562 vertices per hemisphere) was used to balance the vertex resolution and computational cost at individual level. For each participant, we mapped the measurements of cortical thickness and estimates of myelination (T1w/T2w ratio), as provided by the HCP's minimally preprocessing pipeline (Glasser et al., 2013), to the same surface space. Details regarding the HCP dataset and minimal preprocessing pipeline are published in prior studies (Glasser et al., 2013; Smith et al., 2013). We also generated the group-averaged connectivity matrix, via the arithmetic mean of the individual connectivity matrices, using this subset to replicate the group-level results for both GSR and non-GSR data.

In addition, we replicated our findings in a cross-sectional lifespan sample with 313 healthy participants (214 female, age: 6–85 years, 42.2 ± 22.4 years) selected from the NKI-RS dataset, who have no diagnosis of any mental or neurological disorders and passed quality control of a head motion criteria (mean framewise displacement < 0.25 mm). The NKI-RS data was acquired at the Nathan Kline Institute on a Siemens TrioTim 3 Tesla scanner using a multiband sequence. Resting-state fMRI was acquired with a multiband factor of 4, 3 mm isotropic resolution, and a repetition time of 0.645 s for a duration of 9.7 min, which resulted in 900 vol per run. Preprocessing was performed with the Connectome

Table 1
Analytic Workflow; HCP - Human Connectome Project; NKI-RS - Nathan Kline Institute Rockland Sample; GSR - Global Signal Regression; FSIQ - Full Scale Intelligence Quotient.

Objective	Analytic Method	Datasets	Finding
Sort connections based on strength and systematically compare principal gradients calculated using equally sized subsets (i.e., bins) defined based on their strengths	PCA gradients	HCP dense connectome, HCP 100 unrelated subjects (GSR, no GSR)	(Only) the principal gradient is omnipresent in the functional connectome across different connectivity bins
Find coherent regions characterized by principal gradients across differing connectivity strength bins	k-means Clustering	HCP dense connectome, HCP 100 unrelated subjects (GSR, no GSR)	The clustering reflects cortical hierarchy and individual anatomy
Measure inter-bin agreement of individual differences in the principal gradients (vertex-level, cortex-level)	Discriminability, Intraclass Correlation, Spatial Correlation	HCP 100 unrelated subjects (GSR, no GSR)	The principal gradients of the connectome at intermediate strength bins capture individual differences
Assess relative predictive value of principal gradients calculated using differing connectivity strength bins (individually and collectively) (dependent variables: age, sex, FSIQ)	Logistic Regression, Ridge Regression	NKI-RS 313 individuals (GSR, no GSR)	Principal gradients of intermediate connectivity strength bins can individually and collectively improve predictive modeling

Computational System (Xu et al., 2015), and included discarding the first five timepoints, compressing temporal spikes (AFNI 3dDespike), slice timing correction, motion correction, 4D global mean intensity normalization, nuisance regression (Friston's 24 model, cerebrospinal fluid and white matter), linear and quadratic detrending, as well as bandpass filtering (0.01–0.1 Hz). Preprocessing steps were repeated to include GSR and non-GSR respectively. The preprocessed data were then projected on the fsaverage surface, and similarly to the HCP dataset downsampled to the fsaverage4 surface. Details of the dataset and preprocessing were described in our prior studies (Nenning et al., 2020; Nooner et al., 2012). We used Pearson's correlation to establish the individual connectivity matrices for both GSR and non-GSR data.

2.2. Connectivity gradients

The common connectivity gradient approach is based on a functional connectivity matrix that is thresholded vertex-wise (i.e., row-wise), characterizing only the strongest, positive connectivity structure (Margulies et al., 2016). For each vertex, the threshold (ε-neighborhood) retaining only the 10% strongest positive connections can be denoted as a connectivity bin $[\varepsilon_{Lower},\varepsilon_{Upper}]$, where ε_{Lower} is the 90th and ε_{Upper} the 100th connectivity percentile. Subsequently, cosine distance is used to establish a similarity matrix, representing the spatial similarity of the functional connectivity patterns between all vertices with weights ranging from 0 (no similarity) to 1 (high similarity). This similarity matrix is then used in a manifold learning algorithm of choice to characterize the so-called connectivity gradients.

Here, we make two adjustments to this approach, primarily in the graph thresholding step. First, we modify the requirement for the 10% strongest, positive connections and vary the connectivity threshold $[\varepsilon_{Lower},\varepsilon_{Upper}]$ for each vertex. The lower connectivity threshold ε_{Lower} is chosen between the 0th and 90th percentile, and the upper threshold ε_{Upper} is defined as the $(\varepsilon_{Lower}+10)^{th}$ percentile. Second, because low-ranked connectivity bins can comprise negative connectivity weights, we binarize the thresholded connectivity matrix by setting all the retained positive or negative connections to 1 and 0 otherwise. This will emphasize the topography of the thresholded connectivity structure at relative connectivity ranks rather than absolute correlation values. Finally, a similarity matrix is established by calculating the vertex-wise cosine distance of this thresholded binary connectivity matrix.

To establish the low-dimensional representations, i.e., connectivity gradients, we used Principal Component Analysis (PCA) of the similarity matrix, because PCA showed an improved reliability and predictive validity compared to other manifold learning approaches (Hong et al., 2020). An overview of the connectivity gradient workflow is shown in Fig. 1.

Gradient analysis of the high-resolution HCP dense group-average connectome (91,282 grayordinates) requires a large amount of computational resources and is often infeasible on a standard computational infrastructure. Following previous work (Kong et al., 2019; Yeo et al., 2011), instead of calculating the pair-wise connectivity profiles for each grayordinate, we defined the connectivity profiles as the correlation of each grayordinate to 1049 landmark regions of interest (ROIs). These landmark ROIs were defined by a functional cortical parcellation into 998 regions (Schaefer et al., 2018) (2 ROIs of 1000 were not covered by the dense connectome), 17 subcortical structures (Patenaude et al., 2011), and 34 cerebellar ROIs (Buckner et al., 2011). Thus, the HCP dense group-average connectome was expressed by a 91,282×1049 matrix. To establish the similarity matrix, we first calculated a 1049×1049 connectivity matrix between all ROIs, referred to as region-wise connectivity matrix. We then calculated the cosine distance between the thresholded connectivity profiles and the thresholded region-wise connectivity matrix. This resulted in a similarity matrix of size 91,282×1049 that was embedded via PCA. Connectivity gradients were simultaneously generated on a vertex-/voxel-level for cortex, subcortex, and cerebellum, resulting in one set of gradients across all the structures. For visualization purposes, the connectivity profiles and their spatial similarity of the symmetric region-wise connectivity matrix is displayed for the dense group connectome. Because of the lower resolution and computational feasibility, for the HCP unrelated 100 and the NKI-RS samples, we followed the common approach without the landmarks and created a full symmetric similarity matrix (Margulies et al., 2016).

2.3. Comparing gradients across the connectivity strength bins

We establish connectivity gradients for different threshold bins $[\varepsilon_{Lower},\varepsilon_{Upper}]$, ranging from the strongest negative correlations to the strongest positive correlations along the connectivity spectrum, by systematically increasing the percentile thresholds ε_{Lower} and ε_{Upper} (defined as the ε_{Lower}+10). To evaluate the order of the connectivity gradients and ensure comparability across the different thresholds, we performed orthogonal Procrustes alignment (Langs et al., 2015; Wang and Mahadevan, 2008). Each threshold-specific embedding was aligned to the individual or group specific reference defined by the conventional gradients based on the vertex-wise connectivity threshold of the $[90,100]^{th}$ percentile bin (Margulies et al., 2016). Orthogonal Procrustes finds the optimal linear transformation so that two sets of gradients are matched, reflecting the component order and their similarity in the transformation matrix. The component order is informative for the occurrence of specific connectivity gradients and their relative variance explained.

After Procrustes alignment, we examined the cross-threshold changes of the gradient across the brain. To test which brain regions

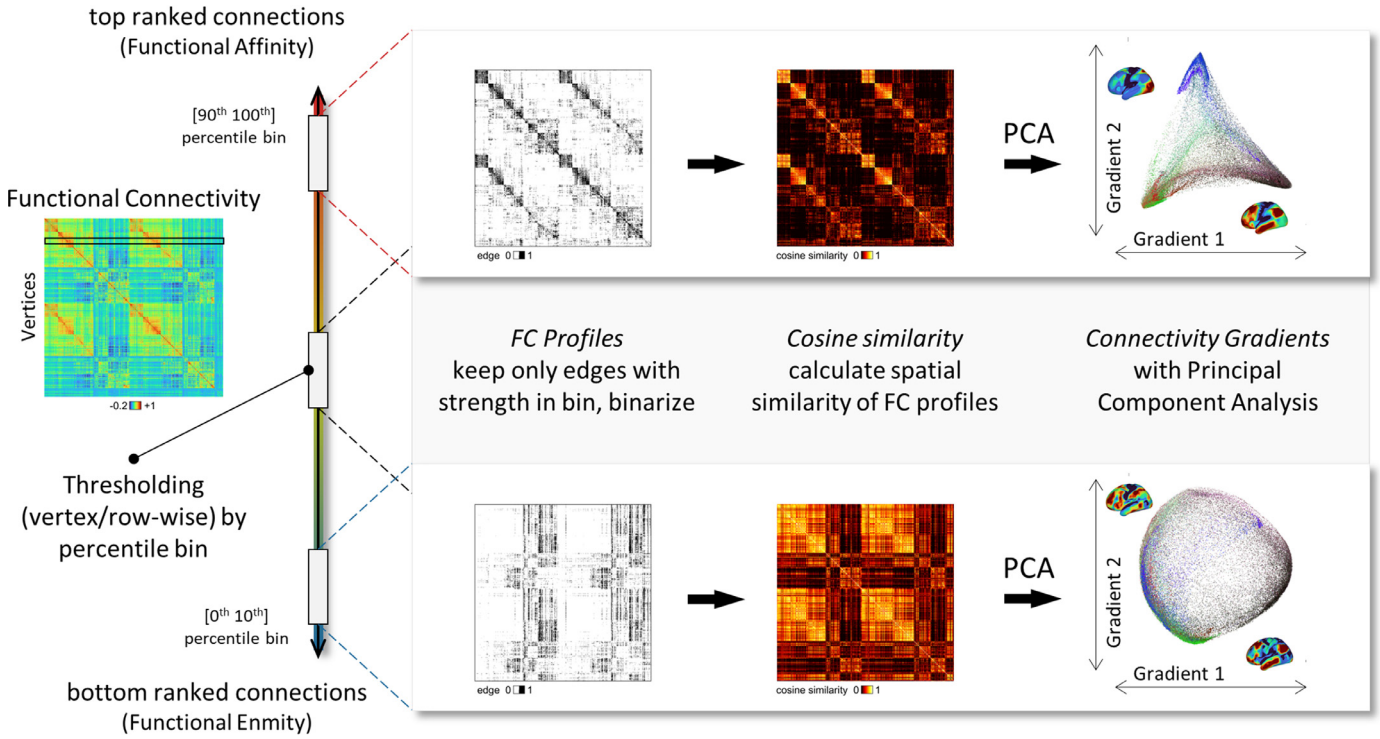

Fig. 1. Overview of the connectivity gradient workflow. In contrast to keeping only the strongest connections, the functional connectivity structure is vertex-wise (row-wise) thresholded based on a defined percentile bin with lower and upper boundary. This results in functional connectivity (FC) profiles with specific subsets of connections that are systematically defined based on their functional connectivity strengths. A similarity matrix is established by the vertex-wise cosine distance of this thresholded and binarized connectivity matrix. Principal component analysis (PCA) is then applied to this similarity matrix to establish a percentile bin-specific embedding and connectivity gradients.

share the similar gradient scores across thresholds, we concatenated the threshold-specific gradients and used k-means clustering to partition the brain into three regions that have a similar pattern of variation across thresholds.

2.4. Reliability and the ability to identify individuals

To quantify reliability of the principal gradients for each threshold, we used 2 repeated resting-state acquisitions from 100 unrelated individuals in the HCP sample. At the global level, discriminability was used to measure how similar an individual's principal gradients are to each other (Bridgeford et al., 2021). Briefly, discriminability is a nonparametric multivariate statistic that assesses the degree to which repeated measurements (e.g., gradients of different sessions) of one individual are relatively similar to each other. It is defined as one minus the fraction of times between-individual measurements are more similar than within-individual measurements. An index of 1 indicates a perfect discriminability. At the vertex level, we quantified the intraclass correlation coefficient (ICC) (Shrout and Fleiss, 1979), a univariate measure of the degree of absolute agreement, for each threshold. ICC is defined as the ratio of between-individual variation divided by the sum of within-individual and between-individual variation. Similarly, we also used ICC to measure the reliability of the gradients between thresholded connectivity bins. We chose discriminability because it is a nonparametric multivariate statistic, and ICC because it is well established in the field of neuroimaging and can be used to measure the agreement between different conditions (Milham et al., 2021; Zuo et al., 2019).

2.5. The predictive potential across connectivity bins

We used 313 individuals from the NKI-RS sample to compare which threshold provides better prediction of individual-specific measures (i.e., age, sex, FSIQ). We performed predictive analyses using the principal gradients of each connectivity strength bin as features, as well as all threshold-specific gradients combined as a feature ensemble. To reduce the feature dimensionality, we used the HCP multimodal parcellation (Glasser et al., 2016) and summarized the gradient coefficients as the average of all the vertices in each of the 360 ROIs. We used ridge regression to predict age and FSIQ, and logistic regression to classify sex, both with a L2 regularization to combat overfitting. Both prediction tasks were performed using glmnet (Friedman et al., 2010) and a nested 10-fold cross-validation scheme for hyperparameter (lambda) selection. The prediction of each fold was aggregated, and we reported accuracy for sex classification and mean absolute error (MAE) for age and FSIQ prediction. To test whether the predictions are significantly greater than chance, we also performed the same predictive modeling procedures 500 times with randomly shuffled labels.

3. Results

3.1. A similar principal gradient for top- and bottom-ranked functional connections

First, we compared the principal gradients of the most opposing functional connectivity structures, defined by the 10% top-ranked connections (functional affinity), and the 10% bottom-ranked connections (functionally enmity). For both functional affinity and the converse functional enmity, the low-dimensional embedding resulted in a similar principal gradient representation across the cortex (r = 0.84), the cerebellum (r = 0.88), hippocampus (r = 0.86), thalamus (r = 0.94), and striatum (r = 0.86) (Fig. 2). While the thresholded FC profiles had an opposing connectivity structure, their spatial similarities revealed a similar pattern of relationships (r = 0.61) (see also Fig. 3A second row). For both functional affinity and functional enmity, the principal gradient ex-

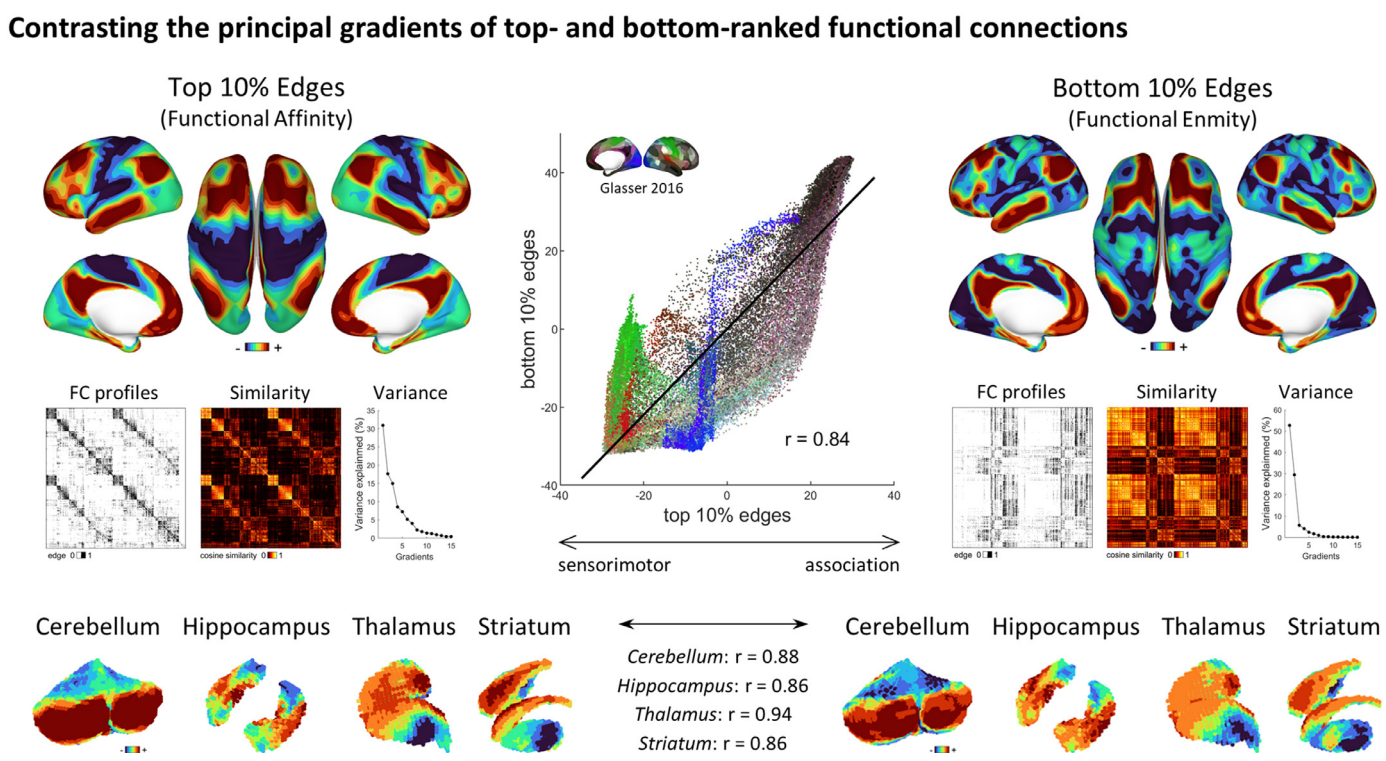

Fig. 2. Similar principal gradients are observed for the top-ranked connections (functional affinity) and the opposing bottom-ranked connections (functional enmity). The thresholded functional connectivity (FC) profiles demonstrate a clear converse functional topography, while their intrinsic similarity structures exhibit a relatively common organizational pattern. The principal gradients in both cortex and subcortex exhibit a high spatial similarity ($r >= 0.84$).

plained the most variance by a clear margin, suggesting a distinct and global characteristic of its spatial pattern. Particularly for the default mode network (DMN), situated on the apex of the principal gradients for both thresholded connectomes, the conjunction of a strong interconnectedness and a coherent segregation from other networks indicated a "common friends, common enemies" analogy.

3.2. The principal gradient is omnipresent across different connectivity thresholds

In a next step, we sought to explore the principal gradient of the connectome at varying connectivity bins, ranging from functional affinity (i.e., the top ranked connections) to functional enmity (i.e., the bottom ranked connections). For all connectivity thresholds, we observed that the sensorimotor-association axis (SA-axis) constitutes the principal gradient (Figs. 3A; S1; Video 1). While the thresholded connectivity profiles showed a transition between the opposing connectivity structures, their intrinsic similarity structures demonstrated a shared pattern of coherence across all the different connectivity strengths (Fig. 3A). Comparable spatial similarities between the threshold-specific principal gradients were observed with and without Procrustes alignment respectively (mean increase in Spearman's ρ after Procrustes = 0.0552 ± 0.0588). The SA-axis was also observed as the principal gradient of a graph composed of vertex-wise similarity profiles from random connectivity bins (i.e. randomized connectivity strength thresholds $[\epsilon_{Lower}, \epsilon_{Upper}]$), emphasizing the shared intrinsic similarity structure across connectivity strengths (Fig. S2). The omnipresence of the principal gradient was evident as well for graphs thresholded at a global correlation value (Fig. S3), group connectomes established with and without global signal regression (Fig. S4), and when using the diffusion map approach (Fig. S5), demonstrating that the observation is robust across common methodological approaches. We also confirmed that this finding is not a construction by the algorithm. We examined the case of a random network and found that the principal gradient is not similar across thresholds (Fig. S6A). Intriguingly, only in the real network data we observed a comparable pattern of spatial similarities between the thresholded connectivity profiles, indicating a similar connectivity structure of integration and segregation that persists across thresholds. Moreover, by evaluating a series of graphs with differing modularity structure, we found that only networks with a two modular structure yield a principal eigenvector that is roughly similar across all thresholds (Fig. S6B). This further strengthens the notion that the SA-axis separates two distinct functional modules that fundamentally shape cortical organization.

The consistency of the topographical pattern encoded by the principal gradients across the connectivity thresholds was underscored by the parameters of the Procrustes alignment (Fig. 3B top row). Importantly, the SA-axis was always the first component of the embedding, i.e., the principal gradient, explaining the most variance. The orthogonal rotation and reflection component T indicated a coefficient consistently close to 1 (abs(T) > 0.85), suggesting similar spatial patterns of the threshold-specific principal gradients and the reference (i.e., based on the strongest 10% connections). A slightly lower similarity and variance explained was observed for intermediate connectivity bins compared to the bottom- and top-ranked ones, reflecting the variation in the principal gradient topography across the connectivity thresholds (Fig. 3B top).

3.3. Only the principal gradient is omnipresent across different threshold bins

Notably, only the principal gradient was found to be omnipresent across different connectivity levels. The second gradient, characterizing an axis between the visual and somatomotor cortex, was not distinctive for low-ranked connections (Fig. 3B middle row; Video 2). It emerged only with increasing connectivity strengths, as reflected in the gradient trajectory maps, but also in the parameters of the Procrustes alignment and variance explained. At bottom-ranked connectivity lev-

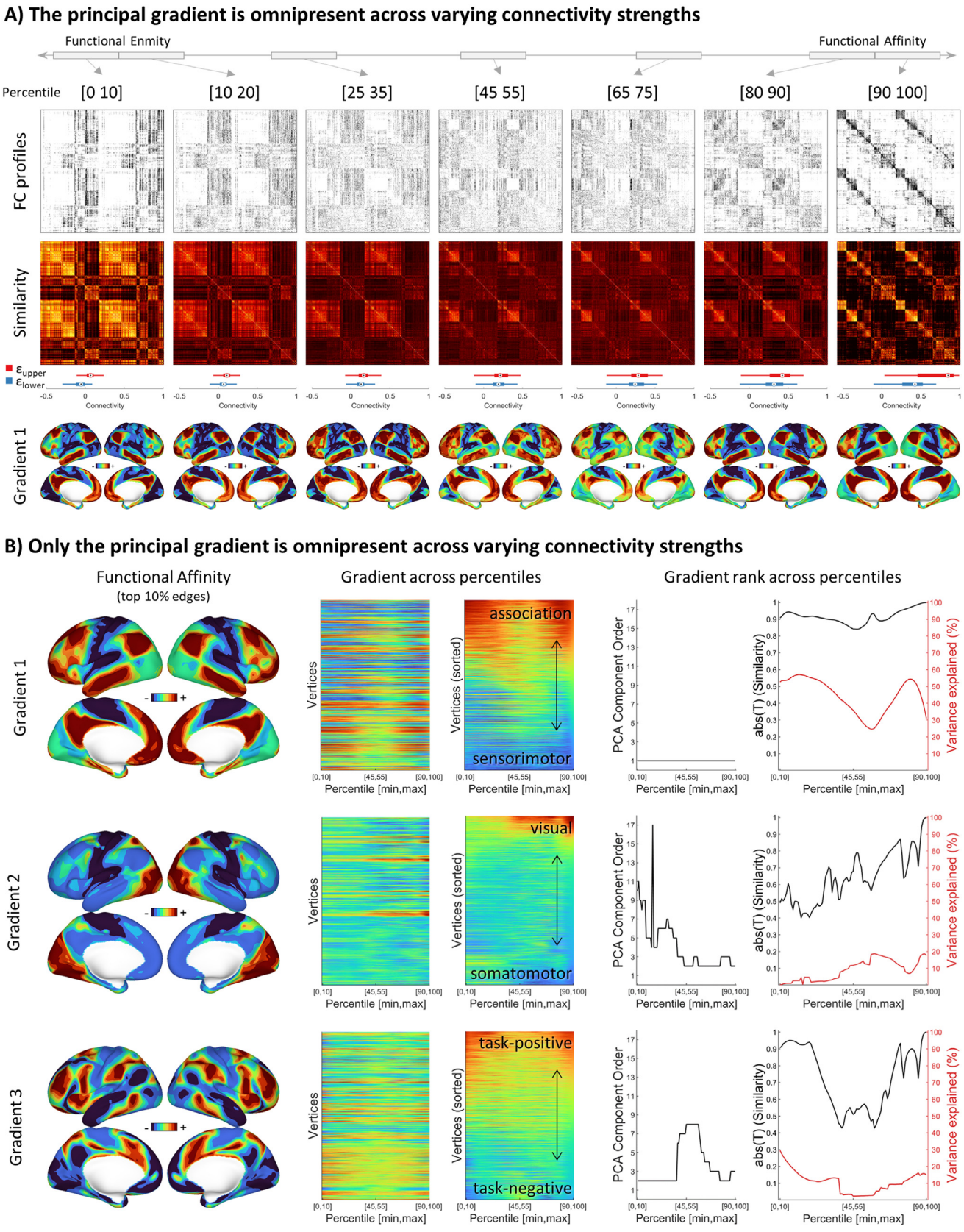

Fig. 3. The sensorimotor-association axis is omnipresent in the functional organization thresholded at different connectivity levels. (A) The thresholded connectivity profiles illustrate a gradual transition between an antagonistic spatial organization, but their intrinsic similarity structures resemble a shared pattern of coherence across the different connectivity levels. (B) Only the principal gradient is omnipresent across the different connectivity thresholds, explaining always the most variance as the first component. The topographical patterns of the somatomotor-visual and task-negative to task-positive gradients vary across the connectivity strengths. The somatomotor-visual gradient emerges only with increasing connectivity strengths, emphasizing its characterization of stronger short-range connections. The task-negative to task-positive gradient describes a similar spatial pattern for the more top- and bottom-ranked connections, but diverges for the intermediate connectivity structure.

els, the second gradient was encoded in trailing components that explained less variance. The third gradient, denoting a transition between task-negative and task-positive regions, showed the highest topographical similarity between low- and top-ranked connectivity bins, but exhibited a deviation for intermediate connections (Fig. 3B bottom row; Video 3). Overall, the variable manifestations of gradients 2 and 3 across the connectivity thresholds emphasize the ubiquitous topography of the principal gradient (Fig. S1). This hints further at the importance of the sensorimotor-association systems as a central feature of functional brain organization.

3.4. Distinct cortical zones are persistent across different connectivity strengths

Next, to probe the consistency of the topographical pattern across differing connectivity bins, we clustered regions based on their changes of the principal gradient profiles. The clusters exhibited a distinct spatial pattern that reflected the two ends of the SA-axis (Fig. 4A). The sensorimotor and association clusters characterize the opposing ends of the connectivity spectrum, separated by an intermediate cluster that can be related to regional variation across the connectivity thresholds (we refer to this as the variable cluster). This transitional cluster layout was also observed in the cerebellum, hippocampus, thalamus, and striatum. The cluster-specific gradient profiles revealed a convergence of the association and the variable clusters at intermediate connectivity strengths (Fig. 4A right).

At the individual level, the clustering was also consistently identified in the HCP sample (Fig. 4B), with and without global signal regression (Fig. S7). The variable cluster showed the largest overlap in attention and limbic networks (Fig. 4B), emphasizing individual differences along the boundaries of the antagonistic association and sensorimotor clusters. Importantly, the cluster configuration was consistent with individual-specific anatomical hierarchies as quantified by cortical myelination (T1w/T2w ratio) and cortical thickness (Fig. 4C). This observation was reproducible with and without global signal regression (Fig. S8). Taken together, the cluster pattern suggested an underlying anatomical principle for the topographic pattern of the principal gradients across the connectivity bins, indicating a non-random configuration of intermediate, variable functional connections.

3.5. Intermediate connections relate to individual microstructure

To characterize the gradient profiles across connectivity bins at the network level, we averaged the gradient scores within canonical resting-state networks. Across connectivity thresholds, the principal gradients reflected the difference between sensory and association cortices, suggesting that this is a relatively stable phenomenon (Fig. 4D). Notably, at intermediate connectivity strengths the gradient scores for the attention networks increased towards gradient scores of high-order networks (i.e., DMN), while the limbic network showed the opposite pattern (Fig. 4D). This finding was also replicated for data processed with and without global signal regression (Fig. S9). At the individual level, we also measured the association between principal gradients and brain microstructure. Notably, intermediate connectivity bins exhibited the strongest (negative) association with a surrogate for myelination (T1w/T2w ratio), and the strongest positive correlation with cortical thickness (Fig. 4E). Similar results were replicated with and without global signal regression, (Fig. S10). The relationship to individual anatomical features, and the increased integration of attention networks into the association cortex (i.e. the closer proximity between both on the gradient spectrum) indicated that the principal gradient of intermediate connections describes an individual-specific functional topography. To unravel why the principal gradients at intermediate connections are more aligned with individual anatomy, we iteratively excluded each vertex from the microstructure-gradient correlation and quantified the resulting change in the relationship. Intriguingly, the difference between the gradient coefficients of intermediate and top-/bottom-ranked connections overlapped with vertices that are relevant for the improved microstructure-gradient correlation at intermediate thresholds (Fig. S11).

3.6. The principal gradients of intermediate connections capture individual differences

Next, we used the HCP sample to evaluate the test-retest reliability of the principal gradients at each connectivity bin with discriminability and ICC, which can also reflect the ability to identify individuals. High discriminability was observed for the principal gradients at the top-ranked and intermediate connectivity strengths (Fig. 5A left). ICC also exhibited higher scores at the top-ranked and the relative lower-ranked connectivity levels (Fig. 5A right). Analysis based on data with global signal regression showed similar results, with an overall higher discriminability across all thresholds, but a drop in the ICC at intermediate levels (Fig. S12A). In addition, we also evaluated the cross-threshold agreement of the principal gradients using ICC. We observed a robust similarity of the principal gradients between top- and bottom-ranked connections calculated on the same data (Fig. 5B left). This observation was also confirmed across test-retest sessions using the HCP sample (Fig. 5B right). Similar results are replicated with data based on global signal regression (Fig. S12B). Taken together, the strong ability to identify individuals, and the individuality of the principal gradients of more loosely coupled connections suggested that they may provide greater information about the individual than their more deterministic counterparts.

3.7. The principal gradients of intermediate connections can improve predictive modeling

The preceding results suggested valuable features in the topography of connectivity levels apart from the strongest connections. To interrogate this notion further, we conducted prediction analyses to evaluate the relative prognostic value of the principal gradient across different connectivity strengths. In a 10-fold cross-validation scheme, we predicted sex, age, and FSIQ based on the principal gradient of each individual connectivity threshold bin, and additionally using all bin-specific gradients combined as a feature ensemble. Of note, we did not aim for the best predictive performance for the phenotypic data, but rather sought to compare the relative predictive power across different connectivity thresholds. For all three prediction tasks, the best performance was achieved with a feature ensemble (i.e., gradients across all thresholds combined) (Fig. 5C, D). The individual bin-specific principal gradients showed mixed performances for the individual predictions. For sex classification, the bottom- and top-ranked connectivity bins had the highest accuracy of 0.68, with only little loss in performance across the individual thresholds (accuracy 0.63–0.67). For age prediction, the principal gradients of the strongest connections achieved the best performance, in terms of lowest mean absolute error, by a clear margin (MAE 14.5y). However, for the prediction of FSIQ, the principal gradients of the more variable bottom-ranked and intermediate connectivity thresholds had the best performance (MAE 10.54 FSIQ points). All predictions were greater than chance (true values always performed better than the null distribution based on shuffled labels), and similar observations were made for principal gradients based on global signal regressed data (Fig. S13). The feature coefficients for all three target variables (i.e., sex, age, FSIQ) and both models (i.e., with and without global signal regression) are displayed in Fig. S14. For the prediction of FSIQ, greater coefficient values were observed in association cortices and default mode network regions at intermediate connectivity thresholds. Reassuringly, these regions have recently been associated with intelligence (Feilong et al., 2021; Hearne et al., 2016; Hilger et al., 2017; Lohmann et al., 2021), and the increase in positive coefficients might explain the benefit of the intermediate connections for predicting FSIQ.

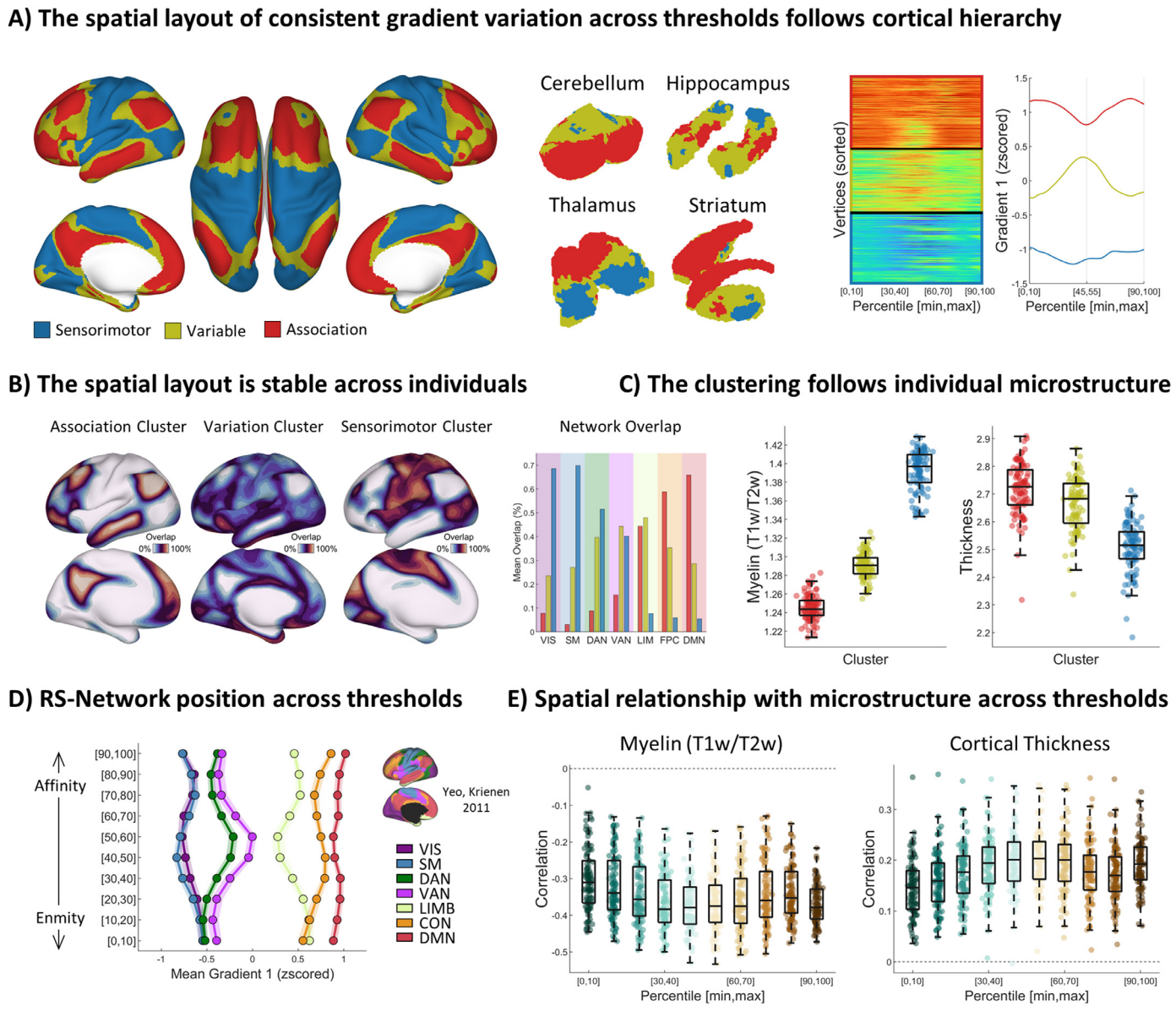

Fig. 4. Clustering of the gradient signatures across the connectivity levels reveals a distinct spatial pattern that reflects cortical hierarchy. (A) The sensorimotor and association cluster, characterizing the opposing ends of the connectivity spectrum, are separated by an intermediate cluster that indicates regional variation across the connectivity thresholds. (A similar spatial cluster pattern is observed for the cortex and in subcortical structures. At intermediate connectivity levels, the gradient coefficients of the association and the variable cluster are more similar. (B) The cluster configuration is repeatedly found across 100 individuals in the HCP sample, with the highest variability in the variable cluster. The variable cluster showed the largest overlap in attention and limbic networks, that are bordering the antagonistic association and sensorimotor clusters. (C) On the individual level, the clustering follows individual microstructural features such as cortical myelination (T1w/T2w ratio) and cortical thickness. (D) At intermediate connectivity levels, the gradient scores of brain regions associated with attention and higher-order networks are more similar, suggesting a stronger integration. (E) Particularly the principal gradients of intermediate connectivity bins are associated with individual microstructure as quantified by cortical myelination (T1w/T2w ratio) and cortical thickness.

4. Discussion

The present work evaluated the specificity and predictive utility of connectivity gradients calculated with differing subsets of connections, which were systematically defined based on their functional connectivity strengths. We demonstrated that regardless of the connection subset examined, the central organizational topography of the principal gradient was reflective of the SA-axis. These findings support the notion that the SA-axis is a fundamental principle of macroscale brain organization. Importantly, however, more loosely coupled connections appear to explain individual differences in anatomy and cognition - in some cases more than stronger connections (e.g., for FSIQ).

Our findings align with converging literature suggesting that the SA-axis is a fundamental principle of large-scale brain organization, capturing patterns of anatomical and functional organization (Huntenburg et al., 2017; Hutchinson and Barrett, 2019; Margulies et al., 2016; Raut et al., 2021; Sydnor et al., 2021). Previous studies have reported that the strongest functional connections place the sensorimotor and association cortices on opposing ends of a connectivity spectrum (Golland et al., 2008; Margulies et al., 2016; Mesmoudi et al., 2013). Notably, our analysis revealed the SA-axis as the principal gradient also across a full range of connectivity thresholds, including connectivity values that can be assumed to describe only intermediate and weak connectivity. This suggests that also the topography of more loosely cou-

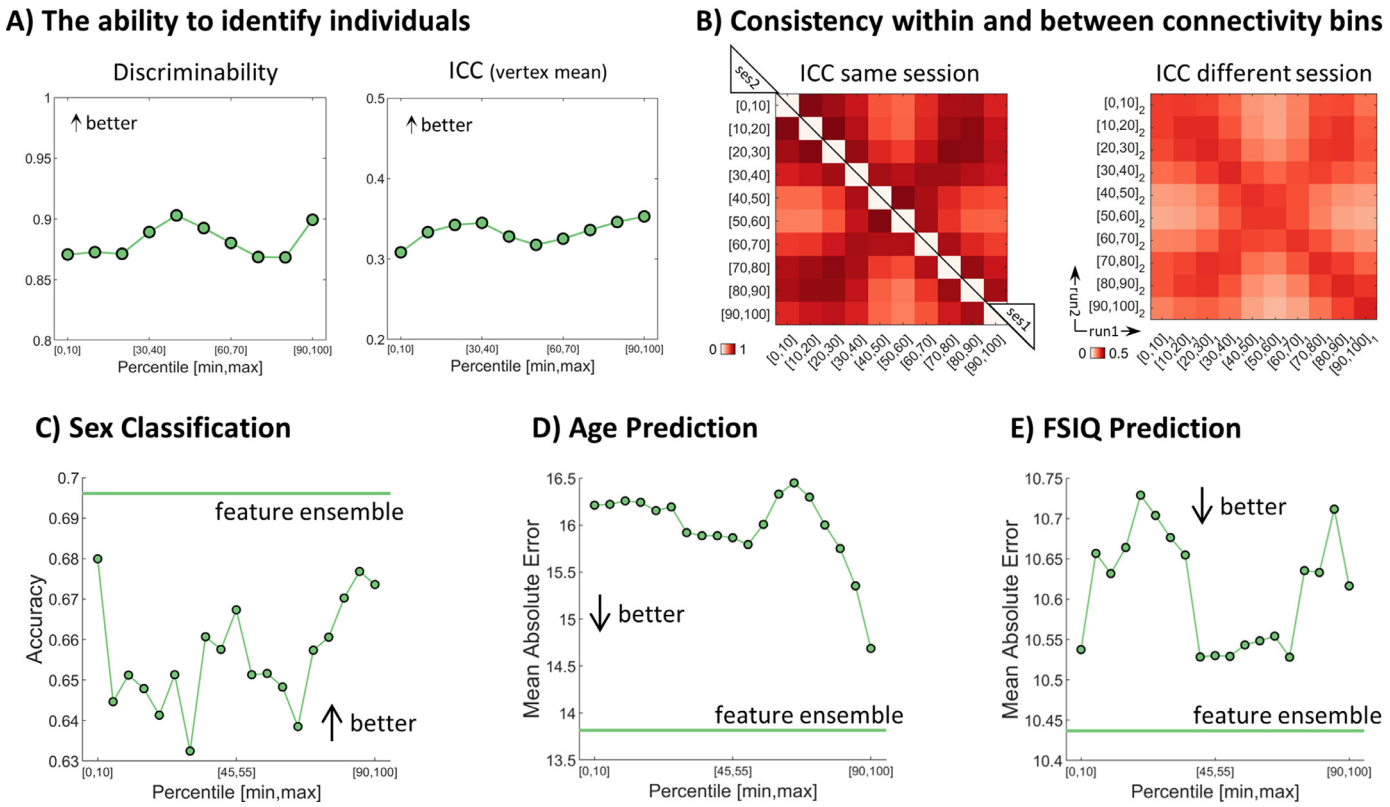

Fig. 5. The principal gradients of intermediate connections capture individual differences, and (A) demonstrate an increased ability to identify individuals. (B) Intraclass correlation between the principal gradients of different connectivity bins emphasizes the distinct topographical patterns of intermediate connections, and their reliability across sessions. C-E) Leveraging the principal gradients of intermediate connections as features can improve the prediction of Sex, Age, and full-scale intelligence quotient (FSIQ).

pled, typically disregarded, connections are not randomly distributed, but are spatially organized along the SA-axis. Previous studies have emphasized the *strength of weak ties* in the functional organization of the brain (Gallos et al., 2012; Goulas et al., 2015; Santarnecchi et al., 2014), and the observed ubiquitous SA-axis could indicate an underlying organizational principle that facilitates efficient information flow in the complex system that the brain is. It is worth noting that in our analyses, the intrinsic similarities of connectivity profiles have always resulted in a fully connected graph, regardless of the chosen connectivity level. This interconnectedness across different thresholds could further reflect a more global, underlying organizational principle of the brain that is shaped by relative connectivity ranks rather than connectivity strengths as usually measured with static linear correlation. Also, our findings were similar for data with and without GSR, emphasizing the stability of the relative connectivity ranks in the connectome. It is important to note that GSR changes connectivity values, increasing the amount of negative connections. Thus, here, weaker and intermediate connections refer primarily to connections at more intermediate positions rank-wise along the connectivity spectrum ranging from the most negative to most positive functional connections.

The tendency of the top- and bottom-ranked functional connections to exhibit the greatest similarity in topographical patterns draws attention to the presence of a “common friends - common enemies” organization for the SA-axis. Initially formulated as the *structural balance* theory in the context of complex social networks (Cartwright and Harary, 1956; Facchetti et al., 2011), this phenomenon has recently been used to characterize the stability of functional brain networks (Saberi et al., 2021). The topographical similarity between top- and bottom-ranked connections emphasizes the central position of the SA-axis in the brain’s functional architecture, and attributes it a crucial role for functional integration and segregation - as previously demonstrated for executive function (Pines et al., 2022). Recent work in the area of autism, where an impaired structural balance of resting-state networks was associated with reduced functional integration and segregation (Hong et al., 2019; Moradimanesh et al., 2021), highlights the potential relevance of understanding abnormalities associated with psychiatric illnesses.

In contrast to the SA-axis, the somatomotor-visual and task-negative to task-positive gradients were more variable across connectivity strengths. The somatomotor-visual gradient was not well delineated at lower connectivity thresholds, and only with increased threshold values did the segregation between somatomotor and visual networks along the gradient axis become evident. This emphasizes that this gradient is dependent on stronger, more local connections, which are a key feature of the unimodal cortex (Sepulcre et al., 2010, 2012). Additionally, the task-negative to task-positive gradient appeared similar only at the extremes, while it differed across intermediate connectivity thresholds, underscoring the antagonistic characteristic of these two systems (Fox et al., 2005). Taken together, the diverging representations of other gradients highlight the apparently central nature of the SA-axis in the functional organization of the brain. Our findings suggest that this central role is seemingly the pinnacle of evolutionary and developmental processes that shape the functional organization across lifespan (Bethlehem et al., 2020; Dong et al., 2021b; Larivière et al., 2020b; Nenning et al., 2020; Xia et al., 2022) and species (Huntenburg et al., 2021; Xu et al., 2020).

Despite its omnipresence, the principal gradient showed a pattern of variation across the connectivity strengths that, consistent with previous approaches, delineated both association and sensorimotor clusters (Golland et al., 2008; Mesmoudi et al., 2013). Our analysis revealed a variational cluster that systematically separated them across cortex and subcortex, emphasizing the gradual transition between the apex and nadir of the SA-axis (Margulies et al., 2016; Sydnor et al., 2021). Notably, the cluster configuration followed individual structural features such as myelination (T1w/T2w ratio) and cortical thickness, hinting at an underlying microstructural mechanism for less consistent

connections. At intermediate connections the association cortex and attention networks had more similar gradient coefficients. This indicates an increased integration between higher-order brain regions and their bordering areas, characterizing an individual-specific functional topography. Brain regions with variable connectivity across individuals are typically located on the border of core networks and have been acknowledged to reflect individual differences (Adelstein et al., 2011; Di Martino et al., 2009; Mennes et al., 2010; Seitzman et al., 2019). Our findings reflected this pattern and conceptually extended it with the observation of meaningful variation along the principal gradient across intermediate connectivity thresholds. Also, the spatial pattern of vertices that are relevant for the improved microstructure-gradient correlation at intermediate thresholds closely resembles the topography of intrinsic timescales (Raut et al., 2020). This further suggests that the connectivity structure of more loosely coupled connections is meaningful.

Intriguingly, the variation along network borders also relates to recent portrayals of the spatiotemporal structure of the brain. Specifically, so-called traveling waves, which slowly propagate along the principal gradient from the sensorimotor towards the association cortex, show the highest variability in their propagation dynamics at the boundaries of higher-order brain regions (Raut et al., 2021). These boundaries were also observed in the spatiotemporal patterns that underlie a multitude of static and dynamic connectivity findings (Bolt et al., 2022), - appearing to reflect a transition between two opposing cortical systems (Mennes et al., 2010). On a participant-level, regions in those boundaries are often affiliated with higher-order networks (Seitzman et al., 2019), suggesting an individualized functional topography that shapes the inter-individual variability of functional connectivity (Di Martino et al., 2009; Mueller et al., 2013; Xu et al., 2019). Our findings further this notion, suggesting that intermediate connections shape a pattern of integration and segregation between higher-order networks and their bordering regions. Additionally, more loosely coupled connections might align with the crossover between opposing large-scale anatomical systems that underlie brain organization (Mesmoudi et al., 2013; Seguin et al., 2019).

The predictive modeling analysis reiterated the value and potential utility of intermediate connections and their topographical pattern. Interestingly, we observed only a small variation in the prediction performance across the thresholds, and the best performance was obtained by an ensemble of threshold-specific connectivity features. This suggests there is meaningful information in all threshold-dependent principal gradients, and that a combination thereof can fully exploit their utility to predict individual-level measures. Also, particularly for the challenging task of predicting FSIQ, the principal gradients of intermediate connections had the highest performance, highlighting the relationship between the functional topography characterized by those more lenient thresholds and complex cognitive measures. This challenges the general assumption that loosely coupled connections mainly represent noise and can be omitted without losing valuable information. Also in medicine, a shift towards personalized medicine has increased interest in individual difference measures. Although the potential advantages of more loosely coupled connections for specific clinical use cases remain to be determined, more lenient connectivity thresholds could be clinically meaningful beyond diagnosis. For example, characterizing a more complete individual functional network topography could allow functional connectivity analyses to more reliably support outcome prediction. Alterations in a diseased functional connectome might be driven by more subtle hypo- or hyper-connectivities, apparent only in more loosely coupled connections - which more stringent thresholds could miss.

The principal gradients of intermediate connectivity levels were reliable across sessions and facilitated identifying individuals, which emphasize an individual-specific functional topography characterized by more variable connections. Such individual-specificity of more loosely coupled connections appeared to be anatomically rooted and highly associated with cortical myelination (T1w/T2w ratio) and cortical thickness. While more loosely coupled connections are not the primary drivers of connectivity differentiation, future work may address how their variance relates to low-dimensional representations of the connectome to further characterize phenotypic differences. Taken together, our findings suggest that more loosely coupled connections, although individual-specific and more variable, characterize the integration between higher-order brain networks and their adjacent regions, in particular attention networks, which may be a fundamental principle of complex cognitive functions, underscoring the *strength of weak ties*.

5. Conclusions

The SA-axis is thought to be a fundamental organizational feature of the mammalian brain, and our results support and extend its putative role as a core pillar of cortical organization. The principal gradient demonstrates a ubiquitous topography across connectivity strengths, indicating a “common friends - common enemies” analogy for functional brain networks. Along the SA-axis, principal gradients derived from typically ignored intermediate connectivity strengths are reliable and align with underlying individual differences in anatomy. More importantly, using the functional organization of intermediate connections enhanced the prediction of individual variation in cognitive function, suggesting that it is biologically meaningful and could be used as a potential marker. Future work establishing the utility and limitations of gradients derived from these more loosely coupled connections within the core SA-axis in development, disease, and individual differences appears likely to inform both basic and applied neuroscientific questions.

Data and code availability

The dataset used in this work are publicly available at the Human Connectome Project (https://www.humanconnectome.org) and the enhanced Nathan Kline Institute-Rockland Sample data repository (http://fcon_1000.projects.nitrc.org/indi/enhanced/). The preprocessing code for the NKI data is available at https://github.com/zuoxinian/CCS, the code for discriminability is available at https://github.com/neurodata/discriminability, and for intraclass coefficient at https://github.com/TingsterX/Reliability_Explorer. Glmnet is available at https://glmnet.stanford.edu/index.html.

Declaration of Competing Interest

None.

Credit authorship contribution statement

Karl-Heinz Nenning: Conceptualization, Formal analysis, Methodology, Software, Visualization, Writing – original draft, Writing – review & editing. **Ting Xu:** Conceptualization, Methodology, Writing – review & editing. **Alexandre R. Franco:** Resources, Writing – review & editing. **Khena M. Swallow:** Writing – review & editing. **Arielle Tambini:** Writing – review & editing. **Daniel S. Margulies:** Writing – review & editing. **Jonathan Smallwood:** Writing – review & editing. **Stanley J. Colcombe:** Conceptualization, Funding acquisition, Resources, Writing – review & editing. **Michael P. Milham:** Conceptualization, Funding acquisition, Resources, Writing – review & editing.

Acknowledgements

Parts of this work were funded by the National Institutes of Health NIH Grants R01AG047596: Mapping interindividual variation in the aging connectome, U01MH099059: Longitudinal Discovery of Brain Developmental Trajectories, R01MH094639: Discovery Science of Human Brain Function Across the Lifespan, and R01MH101555: Real-time fMRI Neurofeedback Based Stratification of Default Network Regulation. RF1MH128696: An Alignment Framework For Mapping Brain Dynamics and Substrates of Human Cognition Across Species.

Supplementary materials

Supplementary material associated with this article can be found, in the online version, at doi:10.1016/j.neuroimage.2023.120059.

References

Adelstein, J.S., Shehzad, Z., Mennes, M., Deyoung, C.G., Zuo, X.N., Kelly, C., Margulies, D.S., Bloomfield, A., Gray, J.R., Castellanos, F.X., Milham, M.P., 2011. Personality is reflected in the brain's intrinsic functional architecture. PLoS One 6 (11). doi:10.1371/journal.pone.0027633.

Atasoy, S., Donnelly, I., Pearson, J., 2016. Human brain networks function in connectome-specific harmonic waves. Nat. Commun. 7. doi:10.1038/ncomms10340.

Bethlehem, R.A.I., Paquola, C., Seidlitz, J., Ronan, L., Bernhardt, B., Consortium, C.C., Tsvetanov, K.A., 2020. Dispersion of functional gradients across the adult lifespan. Neuroimage 222. doi:10.1016/j.neuroimage.2020.117299.

Bolt, T., Nomi, J.S., Bzdok, D., Salas, J.A., Chang, C., Bt, T.Y., Uddin, L.Q., Keilholz, S.D., 2022. A parsimonious description of global functional brain organization in three spatiotemporal patterns. Nat. Neurosci. 25 (8). doi:10.1038/s41593-022-01118-1.

Bridgeford, E.W., Wang, S., Wang, Z., Xu, T., Craddock, C., Dey, J., Kiar, G., Gray-Roncal, W., Colantuoni, C., Douville, C., Noble, S., Priebe, C.E., Caffo, B., Milham, M., Zuo, X.N., Vogelstein, J.T., 2021. Eliminating accidental deviations to minimize generalization error and maximize replicability: applications in connectomics and genomics. PLoS Comput. Biol. 17 (9). doi:10.1371/journal.pcbi.1009279.

Brown, J.A., Lee, A.J., Pasquini, L., Seeley, W.W., 2022. A dynamic gradient architecture generates brain activity states. Neuroimage 261. doi:10.1016/j.neuroimage.2022.119526.

Buckner, R.L., Krienen, F.M., Castellanos, A., Diaz, J.C., Yeo, B.T., 2011. The organization of the human cerebellum estimated by intrinsic functional connectivity. J. Neurophysiol. 106 (5). doi:10.1152/jn.00339.2011.

Caciagli, L., Paquola, C., He, X., Vollmar, C., Centeno, M., Wandschneider, B., Braun, U., Trimmel, K., Vos, S.B., Sidhu, M.K., Thompson, P.J., Baxendale, S., Winston, G.P., Duncan, J.S., Bassett, D.S., Koepp, M.J., Bernhardt, B.C., 2022. Disorganization of language and working memory systems in frontal versus temporal lobe epilepsy. Brain A J. Neurol. doi:10.1093/brain/awac150.

Cartwright, D., Harary, F., 1956. Structural balance: a generalization of Heider's theory. Psychol. Rev. 63 (5). doi:10.1037/h0046049.

Cohen, A.L., Fair, D.A., Dosenbach, N.U., Miezin, F.M., Dierker, D., Van Essen, D.C., Schlaggar, B.L., Petersen, S.E., 2008. Defining functional areas in individual human brains using resting functional connectivity MRI. Neuroimage 41 (1). doi:10.1016/j.neuroimage.2008.01.066.

Di Martino, A., Shehzad, Z., Kelly, C., Roy, A.K., Gee, D.G., Uddin, L.Q., Gotimer, K., Klein, D.F., Castellanos, F.X., Milham, M.P., 2009. Relationship between cingulo-insular functional connectivity and autistic traits in neurotypical adults. Am. J. Psychiatry 166 (8). doi:10.1176/appi.ajp.2009.08121894.

Dong, D., Yao, D., Wang, Y., Hong, S.J., Genon, S., Xin, F., Jung, K., He, H., Chang, X., Duan, M., Bernhardt, B.C., Margulies, D.S., Sepulcre, J., Eickhoff, S.B., Luo, C., 2021a. Compressed sensorimotor-to-transmodal hierarchical organization in schizophrenia. Psychol. Med. doi:10.1017/S0033291721002129.

Dong, H.M., Margulies, D.S., Zuo, X.N., Holmes, A.J., 2021b. Shifting gradients of macroscale cortical organization mark the transition from childhood to adolescence. Proc. Natl. Acad. Sci. U. S. A. (28) 118. doi:10.1073/pnas.2024448118.

Facchetti, G., Iacono, G., Altafini, C., 2011. Computing global structural balance in large-scale signed social networks. Proc. Natl. Acad. Sci. U. S. A. 108 (52), 20953.

Feilong, M., Swaroop Guntupalli, J., Haxby, J.V., 2021. The neural basis of intelligence in fine-grained cortical topographies. Elife 10. doi:10.7554/eLife.64058.

Fox, M.D., Snyder, A.Z., Vincent, J.L., Corbetta, M., Van Essen, D.C., Raichle, M.E., 2005. The human brain is intrinsically organized into dynamic, anticorrelated functional networks. Proc. Natl. Acad. Sci. U. S. A. 102 (27), 9673–9678.

Friedman, J., Hastie, T., Tibshirani, R., 2010. Regularization paths for generalized linear models via coordinate descent. J. Stat. Softw. 33 (1). https://pubmed.ncbi.nlm.nih.gov/20808728/.

Gallos, L.K., Makse, H.A., Sigman, M., 2012. A small world of weak ties provides optimal global integration of self-similar modules in functional brain networks. Proc. Natl. Acad. Sci. U. S. A. 109 (8), 2825–2830.

Gee, D.G., Biswal, B.B., Kelly, C., Stark, D.E., Margulies, D.S., Shehzad, Z., Uddin, L.Q., Klein, D.F., Banich, M.T., Castellanos, F.X., Milham, M.P., 2011. Low frequency fluctuations reveal integrated and segregated processing among the cerebral hemispheres. Neuroimage 54 (1). doi:10.1016/j.neuroimage.2010.05.073.

Glasser, M.F., Coalson, T.S., Robinson, E.C., Hacker, C.D., Harwell, J., Yacoub, E., Ugurbil, K., Andersson, J., Beckmann, C.F., Jenkinson, M., Smith, S.M., Van Essen, D.C., 2016. A multi-modal parcellation of human cerebral cortex. Nature 536 (7615), 171–178.

Glasser, M.F., Sotiropoulos, S.N., Wilson, J.A., Coalson, T.S., Fischl, B., Andersson, J.L., Xu, J., Jbabdi, S., Webster, M., Polimeni, J.R., Van Essen, D.C., Jenkinson, M.WU-Minn HCP Consortium, 2013. The minimal preprocessing pipelines for the Human Connectome Project. Neuroimage 80, 105–124.

Glomb, K., Kringelbach, M.L., Deco, G., Hagmann, P., Pearson, J., Atasoy, S., 2021. Functional harmonics reveal multi-dimensional basis functions underlying cortical organization. Cell Rep. 36 (8). doi:10.1016/j.celrep.2021.109554.

Golland, Y., Golland, P., Bentin, S., Malach, R., 2008. Data-driven clustering reveals a fundamental subdivision of the human cortex into two global systems. Neuropsychologia 46 (2), 540.

Gordon, E.M., Laumann, T.O., Gilmore, A.W., Newbold, D.J., Greene, D.J., Berg, J.J., Ortega, M., Hoyt-Drazen, C., Gratton, C., Sun, H., Hampton, J.M., Coalson, R.S., Nguyen, A.L., McDermott, K.B., Shimony, J.S., Snyder, A.Z., Schlaggar, B.L., Petersen, S.E., Nelson, S.M., Dosenbach, N.U.F., 2017. Precision functional mapping of individual human brains. Neuron 95 (4), 791.

Goulas, A., Schaefer, A., Margulies, D.S., 2015. The strength of weak connections in the macaque cortico-cortical network. Brain Struct. Funct. 220 (5), 2939–2951.

Granovetter, M.S., 1973. The strength of weak ties. Am. J. Sociol. 78 (6), 1360–1380.

Guell, X., Schmahmann, J.D., Gabrieli, J., Ghosh, S.S., 2018. Functional gradients of the cerebellum. eLife 7, e36652. doi:10.7554/eLife.36652.

Haak, K.V., Marquand, A.F., Beckmann, C.F., 2018. Connectopic mapping with resting-state fMRI. Neuroimage 170. doi:10.1016/j.neuroimage.2017.06.075.

HCP 1200 Subjects Data Release Reference Manual. (2017). https://www.humanconnectome.org/storage/app/media/documentation/s1200/HCP_S1200_Release_Reference_Manual.pdf

Hearne, L.J., Mattingley, J.B., Cocchi, L., 2016. Functional brain networks related to individual differences in human intelligence at rest. Sci. Rep. 6. doi:10.1038/srep32328.

Hermundstad, A.M., Bassett, D.S., Brown, K.S., Aminoff, E.M., Clewett, D., Freeman, S., Frithsen, A., Johnson, A., Tipper, C.M., Miller, M.B., Grafton, S.T., Carlson, J.M., 2013. Structural foundations of resting-state and task-based functional connectivity in the human brain. Proc. Natl. Acad. Sci. U. S. A. 110 (15). doi:10.1073/pnas.1219562110.

Hilger, K., Ekman, M., Fiebach, C.J., Basten, U., 2017. Intelligence is associated with the modular structure of intrinsic brain networks. Sci. Rep. 7 (1). doi:10.1038/s41598-017-15795-7.

Honey, C.J., Kötter, R., Breakspear, M., Sporns, O., 2007. Network structure of cerebral cortex shapes functional connectivity on multiple time scales. Proc. Natl. Acad. Sci. U. S. A. 104 (24). doi:10.1073/pnas.0701519104.

Honey, C.J., Sporns, O., Cammoun, L., Gigandet, X., Thiran, J.P., Meuli, R., Hagmann, P., 2009. Predicting human resting-state functional connectivity from structural connectivity. Proc. Natl. Acad. Sci. U. S. A. 106 (6). doi:10.1073/pnas.0811168106.

Hong, S.J., de Wael, R.V., Bethlehem, R.A.I., Lariviere, S., Paquola, C., Valk, S.L., Milham, M.P., Di Martino, A., Margulies, D.S., Smallwood, J., Bernhardt, B.C, 2019. Atypical functional connectome hierarchy in autism. Nat. Commun. 10 (1). doi:10.1038/s41467-019-08944-1.

Hong, S.J., Xu, T., Nikolaidis, A., Smallwood, J., Margulies, D.S., Bernhardt, B., Vogelstein, J., Milham, M.P., 2020. Toward a connectivity gradient-based framework for reproducible biomarker discovery. Neuroimage 223, 117322.

Huntenburg, J.M., Bazin, P.-L., Goulas, A., Tardif, C.L., Villringer, A., Margulies, D.S., 2017. A systematic relationship between functional connectivity and intracortical myelin in the human cerebral cortex. Cereb. Cortex 27 (2), 981.

Huntenburg, J.M., Bazin, P.L., Margulies, D.S., 2018. Large-scale gradients in human cortical organization. Trends Cogn. Sci. (Regul. Ed.) 22 (1). doi:10.1016/j.tics.2017.11.002.

Huntenburg, J.M., Yeow, L.Y., Mandino, F., Grandjean, J., 2021. Gradients of functional connectivity in the mouse cortex reflect neocortical evolution. Neuroimage 225, 117528.

Hutchinson, J.B., Barrett, L.F., 2019. The power of predictions: an emerging paradigm for psychological research. Curr. Dir. Psychol. Sci. 28 (3). doi:10.1177/0963721419831992.

Kong, R., Li, J., Orban, C., Sabuncu, M.R., Liu, H., Schaefer, A., Sun, N., Zuo, X.N., Holmes, A.J., Eickhoff, S.B., Thomas Yeo, B.T., 2019. Spatial topography of individual-specific cortical networks predicts human cognition, personality, and emotion. Cereb. Cortex 29 (6), 2533.

Kong, R., Yang, Q., Gordon, E., Xue, A., Yan, X., Orban, C., Zuo, X.N., Spreng, N., Ge, T., Holmes, A., Eickhoff, S., Thomas Yeo, B.T., 2021. Individual-specific areal-level parcellations improve functional connectivity prediction of behavior. Cereb. Cortex 31 (10), 4477.

Langs, G., Golland, P., Ghosh, S.S., 2015. Predicting activation across individuals with resting-state functional connectivity based multi-atlas label fusion. Med. Image Comput. Comput. Assist. Interv. MICCAI Int. Conf. 9350. doi:10.1007/978-3-319-24571-3_38, Med. Image Comput. Comput. Assist. Interv..

Larivière, S., de Wael, R.V., Hong, S.J., Paquola, C., Tavakol, S., Lowe, A.J., Schrader, D.V., Bernhardt, B.C, 2020a. Multiscale structure-function gradients in the neonatal connectome. Cereb. Cortex 30 (1). doi:10.1093/cercor/bhz069.

Larivière, S., de Wael, R.V., Hong, S.J., Paquola, C., Tavakol, S., Lowe, A.J., Schrader, D.V., Bernhardt, B.C, 2020b. Multiscale structure-function gradients in the neonatal connectome. Cereb. Cortex 30 (1). doi:10.1093/cercor/bhz069.

Li, J., Kong, R., Liégeois, R., Orban, C., Tan, Y., Sun, N., Holmes, A.J., Sabuncu, M.R., Ge, T., Yeo, B.T.T., 2019. Global signal regression strengthens association between resting-state functional connectivity and behavior. Neuroimage 196. doi:10.1016/j.neuroimage.2019.04.016.

Li, Q., Tavakol, S., Royer, J., Larivière, S., De Wael, R.V., Park, B.Y., Paquola, C., Zeng, D., Caldairou, B., Bassett, D.S., Bernasconi, A., Bernasconi, N., Frauscher, B., Smallwood, J., Caciagli, L., Li, S., Bernhardt, B.C, 2021. Atypical neural topographies underpin dysfunctional pattern separation in temporal lobe epilepsy. Brain A J. Neurol. 144 (8). doi:10.1093/brain/awab121.

Lohmann, G., Lacosse, E., Ethofer, T., Kumar, V.J., Scheffler, K., & Jost, J. (2021). Predicting intelligence from fMRI data of the human brain in a few minutes of scan time. In *bioRxiv* (p. 2021.03.18.435935). https://www.biorxiv.org/content/10.1101/2021.03.18.435935v1.

Margulies, D.S., Ghosh, S.S., Goulas, A., Falkiewicz, M., Huntenburg, J.M., Langs, G., Bezgin, G., Eickhoff, S.B., Castellanos, F.X., Petrides, M., Jefferies, E., Smallwood, J., 2016. Situating the default-mode network along a principal gradient of macroscale cortical organization. Proc. Natl. Acad. Sci. U. S. A. 113 (44). doi:10.1073/pnas.1608282113.

Markov, N.T., Ercsey-Ravasz, M., Van Essen, D.C., Knoblauch, K., Toroczkai, Z., Kennedy, H., 2013. Cortical high-density counterstream architectures. Science 342 (6158). doi:10.1126/science.1238406.

Meng, Y., Yang, S., Chen, H., Li, J., Xu, Q., Zhang, Q., Lu, G., Zhang, Z., Liao, W., 2021. Systematically disrupted functional gradient of the cortical connectome in generalized epilepsy: initial discovery and independent sample replication. Neuroimage 230. doi:10.1016/j.neuroimage.2021.117831.

Mennes, M., Kelly, C., Zuo, X.-N., Di Martino, A., Biswal, B., Xavier Castellanos, F., Milham, M.P., 2010. Inter-individual differences in resting state functional connectivity predict task-induced BOLD activity. Neuroimage 50 (4), 1690.

Mesmoudi, S., Perlbarg, V., Rudrauf, D., Messe, A., Pinsard, B., Hasboun, D., Cioli, C., Marrelec, G., Toro, R., Benali, H., Burnod, Y., 2013. Resting state networks' corticotopy: the dual intertwined rings architecture. PLoS One 8 (7). doi:10.1371/journal.pone.0067444.

Milham, M.P., Vogelstein, J., Xu, T., 2021. Removing the reliability bottleneck in functional magnetic resonance imaging research to achieve clinical utility. JAMA Psychiatry 78 (6). doi:10.1001/jamapsychiatry.2020.4272.

Moradimanesh, Z., Khosrowabadi, R., Eshaghi Gordji, M., Jafari, G.R., 2021. Altered structural balance of resting-state networks in autism. Sci. Rep. 11 (1), 1–16.

Mueller, S., Wang, D., Fox Yeo, B.T., Sepulcre, J., Sabuncu, M.R., Shafee, R., Lu, J., Liu, H, 2013. Individual variability in functional connectivity architecture of the human brain. Neuron 77 (3). doi:10.1016/j.neuron.2012.12.028.

Mulders, P.C.R., van Eijndhoven, P.F.P., van Oort, J., Oldehinkel, M., Duyser, F.A., Kist, J.D., Collard, R.M., Vrijsen, J.N., Haak, K.V., Beckmann, C.F., Tendolkar, I., & Marquand, A.F. (2022). Association of striatal connectivity gradients to functional domains across psychiatric disorders. In *bioRxiv* (p. 2022.06.02.494510). https://www.biorxiv.org/content/10.1101/2022.06.02.494510v1.

Murphy, K., Fox, M.D., 2017. Towards a consensus regarding global signal regression for resting state functional connectivity MRI. Neuroimage 154, 169.

Nenning, K.H., Liu, H., Ghosh, S.S., Sabuncu, M.R., Schwartz, E., Langs, G., 2017. Diffeomorphic functional brain surface alignment: functional demons. Neuroimage 156. doi:10.1016/j.neuroimage.2017.04.028.

Nenning, K.H., Xu, T., Schwartz, E., Arroyo, J., Woehrer, A., Franco, A.R., Vogelstein, J.T., Margulies, D.S., Liu, H., Smallwood, J., Milham, M.P., Langs, G., 2020. Joint embedding: a scalable alignment to compare individuals in a connectivity space. Neuroimage 222, 117232.

Nooner, K.B., Colcombe, S., Tobe, R., Mennes, M., Benedict, M., Moreno, A., Panek, L., Brown, S., Zavitz, S., Li, Q., Sikka, S., Gutman, D., Bangaru, S., Schlachter, R.T., Kamiel, S., Anwar, A., Hinz, C., Kaplan, M., Rachlin, A., … Milham, M., 2012. The NKI-rockland sample: a model for accelerating the pace of discovery science in psychiatry. Front. Neurosci. doi:10.3389/fnins.2012.00152.

Paquola, C., De Wael, R.V., Wagstyl, K., Bethlehem, R.A.I., Hong, S.J., Seidlitz, J., Bullmore, E.T., Evans, A.C., Misic, B., Margulies, D.S., Smallwood, J., Bernhardt, B.C., 2019. Microstructural and functional gradients are increasingly dissociated in transmodal cortices. PLoS Biol. 17 (5), e3000284.

Park, B.Y., Kebets, V., Larivière, S., Hettwer, Paquola, C., van Rooij, D., Buitelaar, J., Franke, B., Hoogman, M., Schmaal, L., Veltman, D.J., van den Heuvel, O.A., Stein, D.J., Andreassen, O.A., Ching, C.R.K., Turner, J.A., van Erp, T.G.M., Evans, A.C., Dagher, A., … Bernhardt, B.C., 2022. Multiscale neural gradients reflect transdiagnostic effects of major psychiatric conditions on cortical morphology. Commun. Biol. 5 (1). doi:10.1038/s42003-022-03963-z.

Pasquini, L., Fryer, S.L., Eisendrath, S.J., Segal, Z.V., Lee, A.J., Brown, J.A., Saggar, M., Mathalon, D.H., 2022. Dysfunctional cortical gradient topography in treatment-resistant major depressive disorder. Biol. Psychiatry. Cogn. Neurosc. Neuroimaging doi:10.1016/j.bpsc.2022.10.009.

Patenaude, B., Smith, S.M., Kennedy, D.N., Jenkinson, M., 2011. A Bayesian model of shape and appearance for subcortical brain segmentation. Neuroimage 56 (3). doi:10.1016/j.neuroimage.2011.02.046.

Pines, A.R., Larsen, B., Cui, Z., Sydnor, V.J., Bertolero, M.A., Adebimpe, A., Alexander-Bloch, A.F., Davatzikos, C., Fair, D.A., Gur, R.C., Gur, R.E., Li, H., Milham, M.P., Moore, T.M., Murtha, K., Parkes, L., Thompson-Schill, S.L., Shanmugan, S., Shinohara, R.T., … Satterthwaite, T.D., 2022. Dissociable multi-scale patterns of development in personalized brain networks. Nat. Commun. 13 (1), 1–15.

Raut, R.V., Snyder, A.Z., Mitra, A., Yellin, D., Fujii, N., Malach, R., Raichle, M.E., 2021. Global waves synchronize the brain's functional systems with fluctuating arousal. Sci. Adv. 7 (30). doi:10.1126/sciadv.abf2709.

Raut, R.V., Snyder, A.Z., Raichle, M.E., 2020. Hierarchical dynamics as a macroscopic organizing principle of the human brain. Proc. Natl. Acad. Sci. U.S.A. 117 (34). doi:10.1073/pnas.2003383117.

Robinson, E.C., Jbabdi, S., Glasser, M.F., Andersson, J., Burgess, G.C., Harms, M.P., Smith, S.M., Van Essen, D.C., Jenkinson, M., 2014. MSM: a new flexible framework for multimodal surface matching. Neuroimage 100. doi:10.1016/j.neuroimage.2014.05.069.

Saberi, M., Khosrowabadi, R., Khatibi, A., Misic, B., Jafari, G., 2021. Topological impact of negative links on the stability of resting-state brain network. Sci. Rep. 11 (1), 1–14.

Salimi-Khorshidi, G., Douaud, G., Beckmann, C.F., Glasser, M.F., Griffanti, L., Smith, S.M., 2014. Automatic denoising of functional MRI data: combining independent component analysis and hierarchical fusion of classifiers. Neuroimage 90. doi:10.1016/j.neuroimage.2013.11.046.

Samara, A., Eilbott, J., Margulies, D.S., Xu, T., Vanderwal, T., 2023. Cortical gradients during naturalistic processing are hierarchical and modality-specific. NeuroImage, 271, 120023. Advance online publication. doi:10.1016/j.neuroimage.2023.120023.

Santarnecchi, E., Galli, G., Polizzotto, N.R., Rossi, A., Rossi, S., 2014. Efficiency of weak brain connections support general cognitive functioning. Hum. Brain Mapp. 35 (9), 4566.

Schaefer, A., Kong, R., Gordon, E.M., Laumann, T.O., Zuo, X.N., Holmes, A.J., Eickhoff, S.B., Yeo, B.T.T., 2018. Local-global parcellation of the human cerebral cortex from intrinsic functional connectivity MRI. Cereb. Cortex 28 (9). doi:10.1093/cercor/bhx179.

Seguin, C., Razi, A., Zalesky, A., 2019. Inferring neural signalling directionality from undirected structural connectomes. Nat. Commun. 10. doi:10.1038/s41467-019-12201-w.

Seitzman, B.A., Gratton, C., Laumann, T.O., Gordon, E.M., Adeyemo, B., Dworetsky, A., Kraus, B.T., Gilmore, A.W., Berg, J.J., Ortega, M., Nguyen, A., Greene, D.J., McDermott, K.B., Nelson, S.M., Lessov-Schlaggar, C.N., Schlaggar, B.L., Dosenbach, N.U.F., Petersen, S.E., 2019. Trait-like variants in human functional brain networks. Proc. Natl. Acad. Sci. U. S. A. 116 (45). doi:10.1073/pnas.1902932116.

Sepulcre, J., Liu, H., Talukdar, T., Martincorena, I., Thomas Yeo, B.T., Buckner, R.L., 2010. The organization of local and distant functional connectivity in the human brain. PLoS Comput. Biol. 6 (6), e1000808.

Sepulcre, J., Sabuncu, M.R., Yeo, T.B., Liu, H., Johnson, K.A., 2012. Stepwise connectivity of the modal cortex reveals the multimodal organization of the human brain. J. Neurosci. 32 (31), 10649.

Shrout, P.E., Fleiss, J.L., 1979. Intraclass correlations: uses in assessing rater reliability. Psychol. Bull. 86 (2), 420–428.

Smith, S.M., Beckmann, C.F., Andersson, J., Auerbach, E.J., Bijsterbosch, J., Douaud, G., Duff, E., Feinberg, D.A., Griffanti, L., Harms, M.P., Kelly, M., Laumann, T., Miller, K.L., Moeller, S., Petersen, S., Power, J., Salimi-Khorshidi, G., Snyder, A.Z., Vu, A.T.… WU-Minn HCP Consortium, 2013. Resting-state fMRI in the human connectome project. Neuroimage 80, 144–168.

Stark, D.E., Margulies, D.S., Shehzad, Z.E., Reiss, P., Kelly, A.M., Uddin, L.Q., Gee, D.G., Roy, A.K., Banich, M.T., Castellanos, F.X., Milham, M.P., 2008. Regional variation in interhemispheric coordination of intrinsic hemodynamic fluctuations. J. Neurosci. 28 (51). doi:10.1523/JNEUROSCI.4544-08.2008.

Sydnor, V.J., Larsen, B., Bassett, D.S., Alexander-Bloch, A., Fair, D.A., Liston, C., Mackey, A.P., Milham, M.P., Pines, A., Roalf, D.R., Seidlitz, J., Xu, T., Raznahan, A., Satterthwaite, T.D., 2021. Neurodevelopment of the association cortices: patterns, mechanisms, and implications for psychopathology. Neuron 109 (18). doi:10.1016/j.neuron.2021.06.016.

Uğurbil, K., Xu, J., Auerbach, E.J., Moeller, S., Vu, A.T., Duarte-Carvajalino, J.M., Lenglet, C., Wu, X., Schmitter, S., de Moortele, P.F.V., Strupp, J., Sapiro, G., De Martino, F., Wang, D., Harel, N., Garwood, M., Chen, L., Feinberg, D.A., Smith, S.M., … Yacoub, E., 2013. Pushing spatial and temporal resolution for functional and diffusion MRI in the human connectome project. Neuroimage 80. doi:10.1016/j.neuroimage.2013.05.012.

Van Essen, D.C., Smith, S.M., Barch, D.M., Behrens, T.E., Yacoub, E., Ugurbil, K., 2013. The WU-minn human connectome project: an overview. Neuroimage 80. doi:10.1016/j.neuroimage.2013.05.041.

Vos de Wael, R., Benkarim, O., Paquola, C., Lariviere, S., Royer, J., Tavakol, S., Xu, T., Hong, S.J., Langs, G., Valk, S., Misic, B., Milham, M., Margulies, D., Smallwood, J., Bernhardt, B.C., 2020. BrainSpace: a toolbox for the analysis of macroscale gradients in neuroimaging and connectomics datasets. Commun. Biol. 3 (1), 1–10.

Wang, C., Mahadevan, S., 2008. Manifold alignment using procrustes analysis. In: Proceedings of the ICML '08: 25th International Conference on Machine Learning, pp. 1120–1127.

Waymel, A., Friedrich, P., Bastian, P.A., Forkel, S.J., de Schotten, M.T., 2020. Anchoring the human olfactory system to a functional gradient. Neuroimage 216, 116863.

Xia, Y., Xia, M., Liu, J., Liao, X., Lei, T., Liang, X., Zhao, T., Shi, Z., Sun, L., Chen, X., Men, W., Wang, Y., Pan, Z., Luo, J., Peng, S., Chen, M., Hao, L., Tan, S., Gao, J.H., … He, Y., 2022. Development of functional connectome gradients during childhood and adolescence. Sci. Bull. Faculty Agric. Kyushu Univ. 67 (10). doi:10.1016/j.scib.2022.01.002.

Xu, T., Nenning, K.H., Schwartz, E., Hong, S.J., Vogelstein, J.T., Goulas, A., Fair, D.A., Schroeder, C.E., Margulies, D.S., Smallwood, J., Milham, M.P., Langs, G., 2020. Cross-species functional alignment reveals evolutionary hierarchy within the connectome. Neuroimage 223. doi:10.1016/j.neuroimage.2020.117346.

Xu, T., Sturgeon, D., Ramirez, J.S.B., Froudist-Walsh, S., Margulies, D.S., Schroeder, C.E., Fair, D.A., Milham, M.P., 2019. Interindividual variability of functional connectivity in awake and anesthetized rhesus macaque monkeys. Biol. Psychiatry. Cogn. Neurosci. Neuroimaging 4 (6). doi:10.1016/j.bpsc.2019.02.005.

Xu, T., Yang, Z., Jiang, L., Xing, X.X., Zuo, X.N., 2015. A connectome computation system for discovery science of brain. Sci. Bull. Faculty Agric. Kyushu Univ. 60 (1), 86–95.

Yang, Z., Craddock, R.C., Margulies, D.S., Yan, C.G., Milham, M.P., 2014. Common intrinsic connectivity states among posteromedial cortex subdivisions: insights from analysis of temporal dynamics. Neuroimage 93 (Pt 1). doi:10.1016/j.neuroimage.2014.02.014, 0 1.

Yeo, B.T.T., Krienen, F.M., Sepulcre, J., Sabuncu, M.R., Lashkari, D., Hollinshead, M., Roffman, J.L., Smoller, J.W., Zöllei, L., Polimeni, J.R., Fischl, B., Liu, H., Buckner, R.L., 2011. The organization of the human cerebral cortex estimated by intrinsic functional connectivity. J. Neurophysiol. 106 (3), 1125–1165.

Zuo, X.N., Xu, T., Milham, M.P., 2019. Harnessing reliability for neuroscience research. Nat. Hum. Behav. (8) 3. doi:10.1038/s41562-019-0655-x.